The effect of microstructure in the hydrogen embrittlement of a gas pipeline steel

T. ALP
Chemical Engineering Department, King Abdulaziz University, PO Box 9027, Jeddah, Saudi Arabia

B. DOGAN
Canada Centre for Mineral and Energy Technology, Energy, Mines and Resources, Ottawa, Ontario K1A 0G1, Canada

T. J. DAVIES
Department of Metallurgy and Materials Science, UMIST/University of Manchester, Manchester M1 7HS, UK

Hydrogen embrittlement (HE) tests were carried out on a carbon–manganese pipeline steel having a low sulphur content (<0.01%). It was shown that the susceptibility to HE increased as the microstructures changed from ferrite–pearlite to martensite. In the hydrogenated state the fracture surface of the ferrite–pearlite and ferrite–bainite specimens consisted of small cleavage regions surrounding non-metallic (oxide) inclusions; these were called rosettes and were a characteristic feature of the embrittled state. In hydrogenated martensitic specimens, failure was almost entirely intergranular along prior austenite grain boundaries and cracking of martensitic laths. In the martensitic specimens a relationship between inverse time to failure and prior austenite grain size was established.

1. Introduction

The transport of sour gas constitutes a major problem to the pipeline industries. Failures resulting from hydrogen embrittlement and sulphide stress corrosion cracking (SSCC) occur frequently. The selection of steels, and the pertinent thermomechanical treatments for sour gas applications, therefore deserve considerable attention.

It has long been appreciated that the presence of hydrogen in steels increases the susceptibility to hydrogen embrittlement (HE) and hairline cracking and this has become more pronounced with the development of high-strength steels with low (~0.001) sulphur content [1]. Additionally, when hydrogen does not cause embrittlement it is presumed to have migrated to traps, as an intermediate step, and then to gradually escape to the surface. Typical compositions for gas pipeline steels range between 0.08 and 0.15% C, 1.2 and 1.35% Mn, 0.25 and 0.35% Si, and with sulphur less than 0.01%, preferably of the order 0.001 to 0.005%. Microscopic evidence suggests that in these cleaner, high-strength steels the population of sulphide inclusions is very low and they are, therefore, less likely to provide a sufficient number of strong traps for hydrogen so that either hydrogen pressure builds up around the few sulphide particles or alternatively hydrogen may precipitate at other preferred sites.

Although the harmful effects of non-metallic inclusions on fatigue strength and in delayed failure tests is well established, it is often maintained that susceptibility to HE is reduced by increased inclusion content. However, the identification of the "injurious" inclusions and the interaction between the type of inclusion and type of microstructure in a hydrogen-embrittled state is not well established. The microstructural state is particularly important, especially in steels which have been thermomechanically treated to produce high strengths, since it is the microstructural state which controls, to a great extent, those properties such as strength, toughness, ductility and susceptibility to hydrogen-induced embrittlement. A given strength level can be achieved in steels containing different microstructures produced by selective thermomechanical treatments; the resulting toughness, ductility, and particularly the susceptibility to HE do not parallel favourably the strength values [2]. It has been demonstrated unequivocally that the susceptibility to HE is not a function of strength level alone [3–5]. It has been clearly enunciated by Bernstein *et al.* [2] that the practice of "avoiding" embrittlement by producing lower-strength microstructures is not uncommon.

Hobson and Sykes [6] demonstrated that hydrogen-embrittled carbon–manganese steels show a substantial decrease in ductility and true stress at fracture, i.e. fracture occurs at lower levels of strain and a lower fraction of the uncharged stress as the hydrogen content of the steel increases. Furthermore, in high-strength steels, comparatively small hydrogen concentrations produce large changes in true fracture stress and loss of ductility, whereas the changes in lower-strength steels are comparably less.

A major objective of the work reported here was to examine the susceptibility to HE of a gas pipeline

0022–2461/87 $03.00 + .12

steel of 77 $MN\,m^{-2}$ nominal yield strength in the as-received condition. A range of grain sizes, microstructures and strength levels were produced by selective heat treatments. Previous work had shown that hydrogen-induced failures could initiate from such diverse sources as non-metallic inclusions [7] and from martensitic (prior austenite) grain boundaries and martensitic laths [8]; it was also recorded that the micromechanisms of fracture were different in materials having different microstructures. This work was pursued to confirm the microstructural sensitivity to HE of steels having low sulphur contents. It has also been demonstrated that the strength level of a steel alone cannot provide a unique guide to describe its susceptibility to HE.

2. Experimental details

An 18 mm thick plate (supplied by British Steel, Swinden Labs, Sheffield, UK) of X50 steel (0.18 wt % C, 1.27 wt % Mn, 0.34 wt % Si, 0.004 wt % S, 0.019 wt % P) was hot-rolled to a thickness of 4 mm and sections were heat-treated at 900, 1000, 1100, 1200 and 1300° C to achieve a range of grain sizes. After heat treatment specimens were selectively cooled in vermiculite, air and oil-quenched. Standard tensile specimens were blanked out with their long axes parallel to the rolling direction and these were polished parallel to the specimen long axis, finishing on 25 μm diamond and then etched for 15 sec in 2% Nital solution.

Specimens were cathodically charged with hydrogen for 30 min at 100 $A\,m^{-2}$ in 0.4 M sulphuric acid solution poisoned with 5 $mg\,l^{-1}$ of arsenious trioxide. All mechanical tests commenced 5 min after charging to ensure comparability of results. Tensile tests were conducted in an Instron Universal machine using a 10 kg load cell at a crosshead speed of 0.5 $mm\,min^{-1}$; the time to failure, tensile strength and fracture strength were recorded and the reduction of area measured.

Fracture surfaces were examined by optical and scanning electron microscopy and selected areas and inclusions were analysed using an energy-dispersive (EDAX) facility.

3. Results

3.1. The relationship between microstructure, hydrogen embrittlement and mode of fracture

Metallographic and fractographic investigations by optical and SEM examination were carried out on a large number of hydrogenated and unhydrogenated specimens, paying particular attention to the fracture surface characteristics associated with particular microstructural features, including non-metallic inclusions. Optical microscopy showed that the selected combinations of austenitizing temperatures and cooling rates yielded, in general, three distinct types of microstructure. Low austenitizing temperatures coupled with low cooling rates produced microstructures consisting of ferrite and pearlite, while high austenitizing temperatures together with fast cooling rates resulted in lath martensite formation. Intermediate temperatures with moderate rates of cooling gave rise to the formation of ferritic–pearlitic, ferritic–bainitic or bainitic–martensitic microstructures. Increasing the austenitizing temperature led to grain coarsening and, as expected, the ease of martensite formation was enhanced with increasing prior austenite grain size. The banding of the ferrite–pearlite in the as-received rolled plate was replaced by an equiaxed structure after austenitizing; specimens were cut parallel to the rolling direction so that the rectangular cross-section was normal to the rolling direction.

Uncharged specimens, austenitized and cooled slowly in vermiculite, contained predominantly ferrite grains with small amounts of pearlite and exhibited transgranular fracture. The descriptions of the fracture surfaces were confined to examination of the central, flat fracture region. Uncharged specimens showed no evidence of temper-embrittlement; the transgranular fracture was extensively dimpled and non-metallic inclusions were frequently found in the centres of clusters of various-sized dimples. In these uncharged specimens the aspect ratio (height : diameter) of the approximately hemispherical dimples was unity, irrespective of dimple size or the presence of inclusions in dimples. In the hydrogen-embrittled specimens, however, the dimples were shallower, having aspect ratios of 1 : 3 and where dimples contained inclusions the aspect ratio was of the order of 1 : 10. The fracture within the dimples was characteristically cleavage. This feature was often macroscopically distinct and identifiably characteristic of the hydrogen-embrittled state in ferrite–pearlite specimens, and could be counted on a given fracture surface.

These peculiar regions are henceforth referred to as "rosettes" to distinguish them from the more common definition of plastic dimples. A statistical survey showed the rosette density to diminish with increasing grain size, i.e. typically a decrease from 12 rosettes to 2 rosettes per cross-sectional area, with an accompanying change of rosette shape from a shallow profile to a deep pit profile, was readily observable. Almost in all instances rosettes were associated with non-metallic inclusions at their centre. Fig. 1 illustrates a typical fracture surface characterized by rosette formation. The rosettes, generally of elliptical shape, are regions of predominantly brittle fracture with

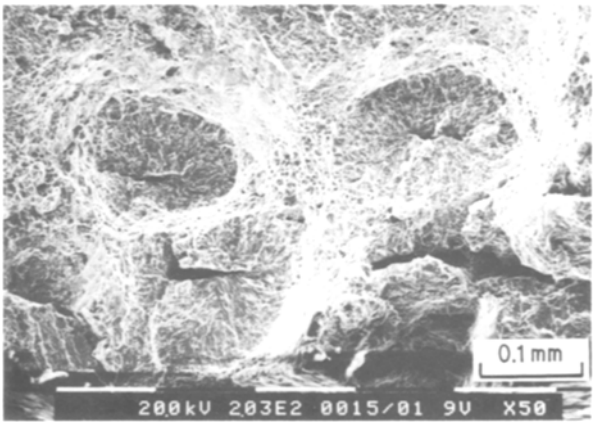

Figure 1 "Rosette" feature in a specimen austenitized at 900° C, vermiculite (V) cooled. Ferrite–pearlite (F/P) microstructure, hydrogen-charged.

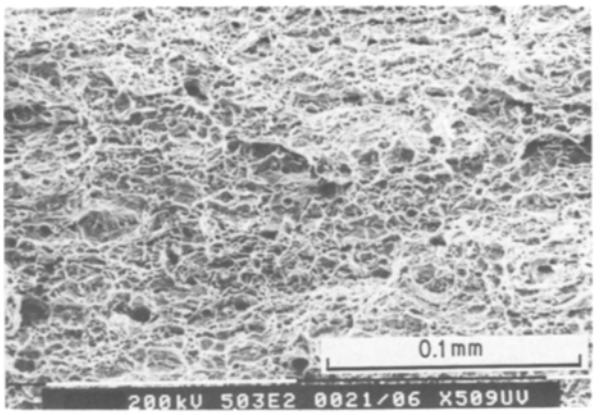

Figure 2 Rolled texture and voids observed on ductile fracture surface of an F/P microstructure specimen, austenitized at 9000° C, vermiculite (V) cooled, uncharged.

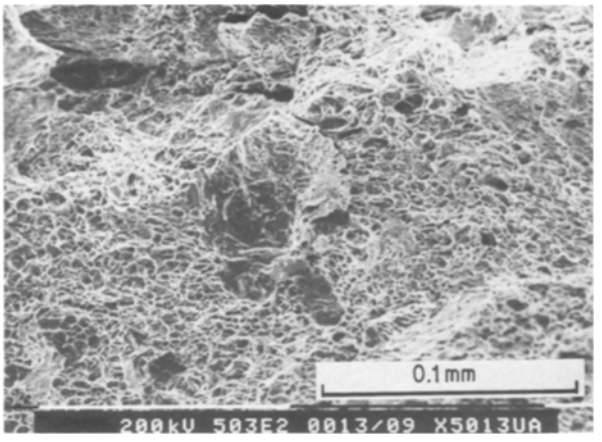

Figure 4 Local cleavage formation in predominantly ductile fracture surface of a bainitic microstructure specimen, austenitized at 1300° C, air (A) cooled, uncharged.

the cleavage tongues advancing radially from the inclusion origin. However, some ductile ridges exist between rosettes and these ridges contain small microvoids similar to those observed in uncharged specimens. These ductile ridges are ostensibly areas of final overload which fail at a high strain rate. The ductility (expressed as percentage reduction in cross-sectional area) was about 60% in uncharged specimens, which was reduced to typically 25% in hydrogenated specimens.

Some minor secondary cracks, parallel to the rolling plane, are thought to be linked to the rolling texture. Fig. 2 depicts fracture surface characteristics observed in the uncharged steel containing ferrite and pearlite. Void formation by debonding at the inclusion–matrix interface is also observed as shown in Fig. 3. A number of these inclusions were analysed in the EDAX attachment on the SEM and were shown to have mixed oxide–silicate compositions containing mainly manganese, iron and aluminium with traces of calcium; these are probably products of the desulphurization and deoxidation reactions.

The specimens having a bainitic microstructure manifest essentially ductile behaviour in the unhydrogenated condition. Fig. 4 shows the fracture surface appearance of a bainitic steel with some pro-eutectoid ferrite at prior austenite grain boundaries. General plasticity, as shown by extensive dimpling, is visible across the whole section. The smaller dimple size, compared to the preceding example, is probably ascribable to the relative lower ductility. The reduction in area obtained in the unembrittled bainitic steel lies in the region of 35%. The micrograph also indicates localized regions of quasi-cleavage. The appearance of certain secondary cracks is indicative of a tendency for transition from a purely transgranular to a mixed mode of failure. Fig. 5 depicts the salient fracture features observed in an essentially bainitic steel in the hydrogen-charged condition. The fracture surface is composed of brittle rosettes and ductile ridges between them. The rosettes do not have well-defined boundaries and are much shallower than in the ferritic–pearlitic embrittled specimens. However, all these regions contain non-metallic inclusions at the centre and the fracture emanates from these inclusions in a cleavage or quasi-cleavage mode, consistent with the loss of ductility (Figs 6 and 7). The measured reduction of area was 10%, i.e. about one-fifth of that of the uncharged state.

The mode of fracture in hydrogenated specimens having a martensitic structure is predominantly brittle. This is evidenced by cleavage and triple-point grain-boundary failures as illustrated in Fig. 8. Some ductility still persists as shown by microvoids between cleavage regions. These microvoids, often non-spherical, contain non-metallic inclusions (Fig. 3).

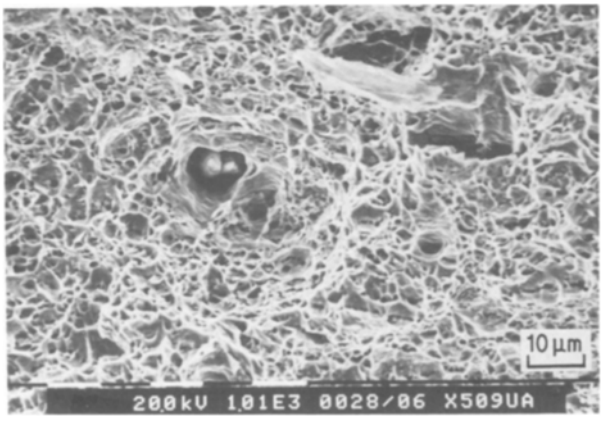

Figure 3 Void formation at inclusions, specimen austenitized at 900° C, air (A) cooled, uncharged.

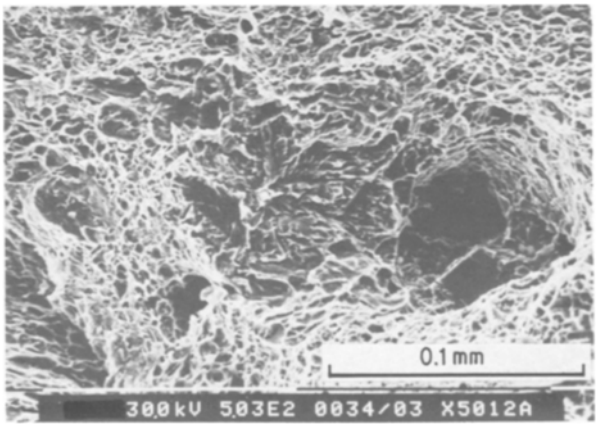

Figure 5 Rosetted fracture surface of a bainitic specimen, austenitized at 1200° C, air (A) cooled, hydrogen-charged. An oxide inclusion is seen in the centre of the rosette.

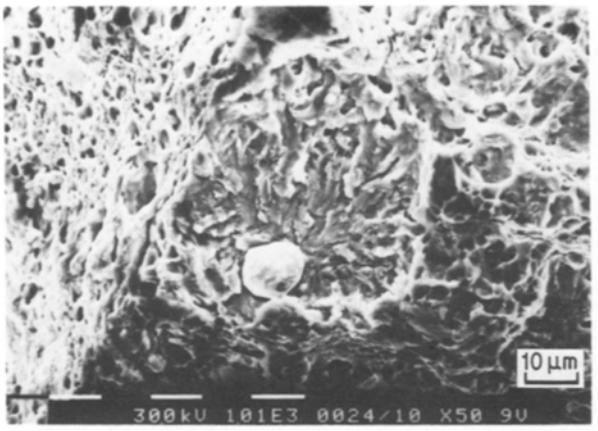

Figure 6 Rosette emanating at an oxide inclusion, specimen austenitized at 1200° C, vermiculite (V) cooled, hydrogen-charged.

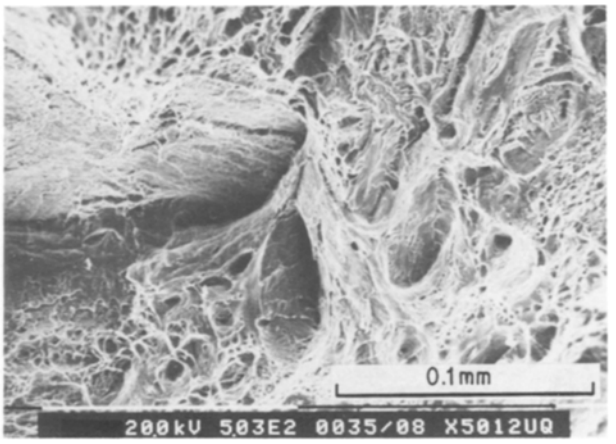

Figure 8 Triple-point fracture of a martensitic specimen and non-spherical voids on a fracture surface, specimen austenitized at 1200° C, oil (O) quenched uncharged.

The martensitic steel exhibited a reduction in area of about 30%. In the hydrogenated condition, mixed modes of fracture were observed, consisting of predominantly flat martensite lath boundary facets linked by small shallow dimples on tear ridges or by raised quasi-cleavage facets. On the grain size level, the major fracture planes were steeply angled with respect to adjacent fracture planes and, particularly noticeable in the large-grained specimens, triple-point boundary cracking and secondary cracking was a common occurrence (Fig. 9). In the specimens of mixed microstructure (containing some bainitic regions) the fracture mode was martensite lath boundary cracking and cleavage with dimpled interconnecting ridges and occasionally some rosette formation.

3.2. Relationships between strength, grain size and time to failure

3.2.1. Martensitic structures

Observations show that, in general, the susceptibility to HE (expressed as a fractional loss of uncharged strength) increased with increasing prior austenite grain size in martensitic structures. This is shown as a straight line with inverse grain size in Fig. 10 where $\sigma_{F_{CH}}/\sigma_{F_U}$ is the ratio of strengths in HE specimens to those in the uncharged specimens and $\bar{d}_\gamma$ is the average prior austenite grain size.

The time taken for these charged martensitic specimens to fail, t_F, is given in Table I. As shown in Fig. 11, a plot of the fractional loss of uncharged strength against inverse time to failure gives a straight-line relationship with a negative slope.

The above relationships may be combined to yield the following relationship between the reduced fracture stress, $\sigma_{F_{CH}}/\sigma_{F_U}$, t_F and $\bar{d}_\gamma$:

$$\frac{\sigma_{F_{CH}}}{\sigma_{F_U}} \propto \frac{1}{t_F}\frac{1}{\bar{d}_\gamma} \quad \text{or} \quad \frac{\sigma_{F_{CH}}}{\sigma_{F_U}} = k\frac{1}{t_F}\frac{1}{\bar{d}_\gamma} \tag{1}$$

where k is a constant. Rearranging Equation 1 gives

$$t_F = k\frac{\sigma_{F_U}}{\sigma_{F_{CH}}}\frac{1}{\bar{d}_\gamma} \tag{2}$$

for the hydrogen-charged martensitic structure. This complementary correspondence between the prior austenite grain size and the inverse time to failure is shown in Fig. 12.

3.2.2. Ferrite–pearlite structures

In ferritic–pearlitic microstructures, and to some

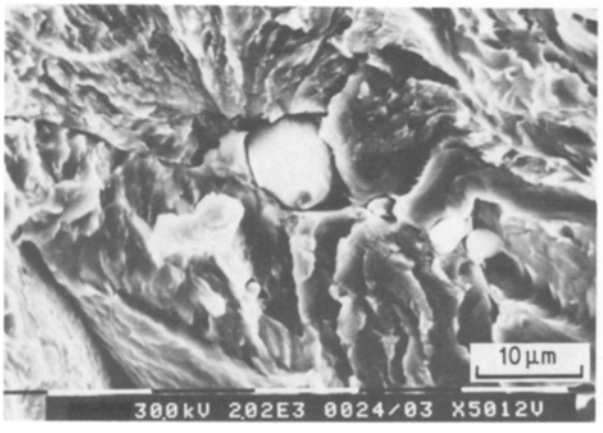

Figure 7 Rosette emanating at an oxide inclusion, specimen austenitized at 1200° C, vermiculite (V) cooled, hydrogen-charged. This electron micrograph shows a similar fracture mode to the coarse-grained specimen.

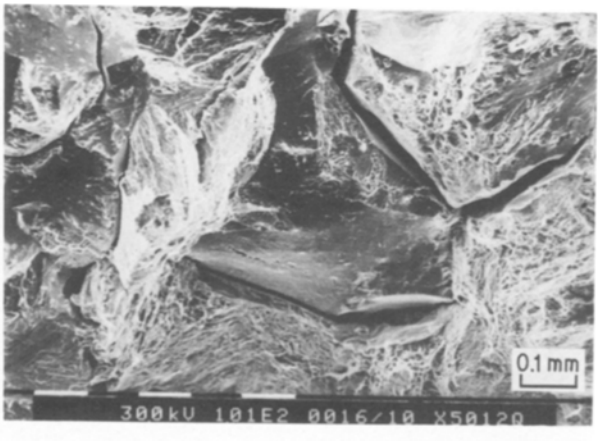

Figure 9 Grain-boundary separation and cleavage fracture in a martensitic specimen, austenitized at 1300° C, oil (O) quenched, hydrogen-charged. The non-metallic inclusions are not fracture initiation sites but are part of the predominant cleavage mode of failure.

TABLE I Catalogue of experimental results

Austenitizing temperature (° C)	Cooling medium*	Microstructure†	Fracture type‡		$\sigma_{F_{CH}}/\sigma_{F_U}$§	$t_{F_{CH}}$ (sec)§	$t_{F_{CH}}/t_{F_U}$§	% RA_{CH}/% RA_U§	$\bar{d}_\gamma$§ (μm)
			Uncharged	Hydrogen-charged					
900	V	F + P	D	D, R	0.67	570	0.67	0.41	9 (F)
	A	F + P	D	D, R	0.71	660	0.83	0.38	6 (F)
	O	F + B	D	D, R (few)	0.55	321	0.38	0.10	5 (F)
1000	V	F + P	D	D, R	0.53	612	0.97	0.29	15 (F)
	A	F + P	D	D, R	0.61	531	0.93	0.25	10 (F)
	O	F + B	D	D, C, R (few)	0.49	254	0.33	0.06	8 (F)
1100	V	F + P	D	D, R	0.60	357	0.53	0.22	100
	A	F + P	D	D, R	0.66	156	0.27	0.24	100
	D	B + M	D	D, C, R	0.44	123	0.21	0.06	100
1200	V	F + P + B	D, C (localized)	D, C, R	0.71	246	0.66	0.35	200
	A	F + B	D, C (localized)	D, C, R	0.61	210	0.45	0.22	200
	O	M	D, C, I (few)	C, I, D (few)	0.28	84	0.28	0.10	300
1300	V	F + P + B	D, C (localized)	D, C, R	0.76	240	0.65	0.54	500
	A	F + B	D, C (localized)	D, C, R (few)	0.87	246	0.57	0.21	500
	O	M	D, C	C, I	0.20	66	0.24	0.13	500

*V, A, O: vermiculite, air, oil quench.

†F, P, B, M: ferrite, pearlite, bainite, martensite.

‡D: ductile, dimpled, transgranular fracture; C, R, I: cleavage fracture, rosettes, intergranular fracture.

§$\sigma_{F_{CH}}/\sigma_{F_U}$: reduced fracture stress; $t_{F_{CH}}$: time to failure (charged condition); $t_{F_{CH}}/t_{F_U}$: reduced time to failure; % RA_{CH}/% RA_U: reduced reduction of area; $\bar{d}_\gamma$: average prior austenite grain size.

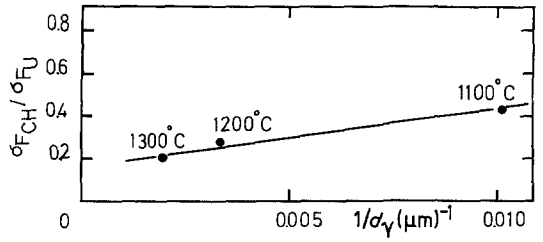

Figure 10 Relationship between reduced fracture stress and inverse prior austenite grain size for martensitic specimens, hydrogen-charged.

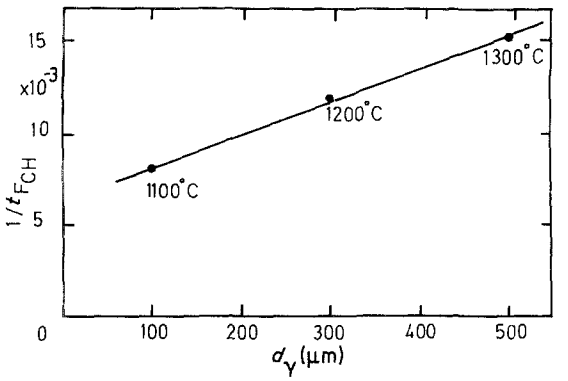

Figure 12 Relationship between inverse time to failure and prior austenite grain size in martensitic structures, hydrogen-charged.

extent in bainitic structures, there is no progressive decrease in the reduced time to failure of hydrogen-charged specimens with increasing grain size. This is shown in Table I, where the reduced failure time $t_{F_{CH}}/t_{F_U}$ ranges between 0.97 and 0.65 (neglecting the 30 μm grain-size material which has a value of 0.53 – this will be commented upon later in relation to all the 1100° C solution-treated specimens). This relative independence of grain size and time to failure is shown by only small changes in the reduced ductility, i.e. a state of almost constant embrittlement of these ferrite–pearlite microstructures.

3.2.3. Solution-treated specimens

The 1100° C solution-treated specimens produce a mixed microstructure consisting of (i) ferrite–bainite with some local regions of martensite (of nominally higher carbon content) in oil-quenched specimens, (ii) ferrite–pearlite with some bainite in air-cooled specimens, and (iii) fine-grained ferrite–pearlite with some Widmanstätten ferrite in the vermiculite-cooled specimens. These mixed microstructures invariably give a low value of the reduced time to failure while not significantly affecting the other physical properties.

4. Discussion

One of the major objectives of this study was to determine whether any significant relationship could be demonstrated (for one steel of given composition) between microstructural features such as phase state, grain size and inclusions and the susceptibility of the steel to HE; the work is not primarily concerned with the atomistic mechanisms involved in crack growth. The fractures are variously described as ductile (e.g. in uncharged ferrite–pearlite structures), cleavage and quasi-cleavage (in mixed microstructures containing some bainite or martensite), and brittle intergranular (mainly in hydrogenated martensitic structures).

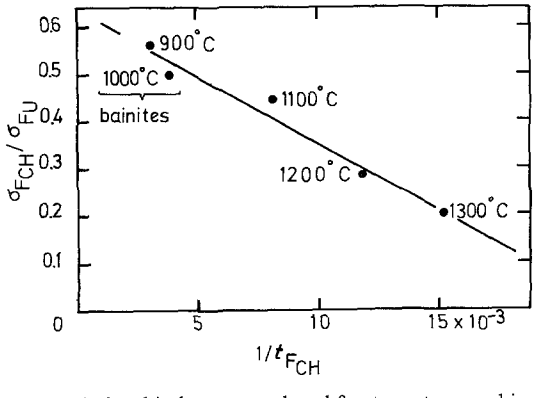

Figure 11 Relationship between reduced fracture stress and inverse time to failure in martensitic specimens, hydrogen-charged.

In addition to the suddenness of the typical HE fracture a major observable and quantifiable effect is the significant loss of ductility compared to the uncharged material in the same microstructural state. The loss of ductility, expressed as a change in fractional reduction of cross-sectional area as given in Table I, shows that the loss of ductility becomes more pronounced as the microstructure changes from ferrite–pearlite to martensite for a given grain size. Additionally as the grain size for a given microstructural state increases by a factor of 100, the loss of ductility does not change significantly. Although the yield strength of ferritic–pearlitic steel is a function of grain size [2], it was shown by Ryder *et al.* [7] that in the HE state microstructure has a more pronounced effect on susceptibility to HE than yield strength; this is also demonstrated by Bernstein and Thompson [9]. These effects are reflected by singular characteristics in the mode of fracture of the different microstructures in the embrittled state. As shown in Fig. 1, the fracture surface of hydrogenated ferrite and pearlite structures consists predominantly of the rosette features described previously, and these invariably contain at least one non-metallic inclusion at their centre; the type of crack is cleavage or quasi-cleavage, emanating from the inclusions which were the origin of fracture in the hydrogenated ferrite– pearlite specimens (Fig. 6).

The different cooling rates produced different microstructures including different size, shape, distribution and coherency of the carbides and non-metallic inclusions [2]. Slow cooling produced large incoherent interfaces around non-metallic inclusions in ferrite–pearlite which provided strong traps for hydrogen; this hydrogen was probably trapped innocuously. These traps are labelled strong or weak, or reversible or irreversible, depending on type and are characterized by their apparent binding energies [10, 11]. From the metallographic records, it was obvious that the non-metallic round, incoherent inclusions are centres of hydrogen and are not as damaging as the fine carbide of the martensite structure. However, these non-metallic inclusions at prior austenite grain boundaries in martensitic structures promote embrittlement by accumulating hydrogen in intrinsically brittle regions; this leads to enhanced

embrittlement [3, 12, 13]. Previous work [14] on the permeation of hydrogen in patented (P) and cold-worked (CW) and tempered martensite structures showed the predominance of weak traps in the tempered martensite structures and strong traps in the cracked carbide of the P and CW structures, thereby providing a reduced susceptibility to HE in the latter.

By contrast, the fracture mode in the mainly martensitic structures was predominantly intergranular, essentially flat fracture with occasional fine dimples and tear ridges linking the brittle regions [15]. These fine dimples are evidence of some local plasticity, probably around a carbide or non-metallic inclusion, which allowed preferential adsorption of hydrogen.

Comparatively high-strength (martensite) and low-strength (ferrite–pearlite) microstructures exhibit a different degree of dimpling. The density of these dimples is significantly less in the martensitic state. This is in agreement with the findings of Thompson and Bernstein [15]. These dimples are evidence of local plastic flow following the fracture of the non-metallic particle–matrix interfaces. If the absorption of hydrogen is facilitated by dislocations in the vicinity of growing cracks [8] then this must be on a local scale in the rosetted specimens. In martensitic steels, cracking occurs along prior austenite grain boundaries and martensite lath boundaries, probably due to (i) adsorption of hydrogen on grain-boundary intersections such as triple points (which is affected by grain size), and (ii) non-metallic inclusions located at prior austenite grain boundaries. The dominance of the brittle intergranular fracture in martensitic specimens compared to the inclusion-sited fracture origins in ferrite–pearlite microstructures is clearly demonstrated in Fig. 9, which shows an inclusion in a martensitic structure; such inclusions are not associated with crack initiation or rosette formation but are incidental features of the intergranular-cleavage fracture surface.

It is interesting to speculate on possible embrittling mechanisms which produce these topographically distinct fracture surfaces. The proposal of Oriani [16] that hydrogen concentrates (precipitates) at regions of high elastic stress is consistent with the inclusion-rosette mode of fracture in ferrite–pearlite structures; this mechanism requires the accumulation of molecular hydrogen at preferred sites (such as inclusion–matrix interfaces) where weakly bound sites exist due to the incoherency and the difference in the coefficients of thermal expansion between the inclusion and the matrix. The local stress criterion would support the observations of cleavage fracture in the rosettes (ferritic–pearlitic structure) and the intergranular failure in the martensitic structures.

In detail, as shown by Lynch [8], the fine-scale microscopy can differ from the macroscopic appearance. The thermodynamic driving force for diffusion of hydrogen to the inclusions is a gradient in chemical potential produced by a gradient in the concentration of lattice hydrogen in the immediate vicinity of the inclusion and/or a gradient in the hydrostatic component of an elastically stressed element [16]. The low chemical potential of the incoherent inclusion–matrix interface provides this gradient, and the concomitant concentration of hydrogen at triaxially stressed regions enhances the gradient and facilitates diffusion; this is a basic feature of delayed failure phenomena in hydrogenated unnotched specimens [7, 14]. The fracture in the rosette surrounding the inclusion is produced by radial cracks growing by cleavage or quasi-cleavage and is thereby consistent with the observation that embrittlement (as described by loss of ductility) is less severe in materials containing these inclusion-initiated failure than in the dominantly grain-boundary failure of the martensitic structures.

The size (i.e. volume) of the rosettes is presumably affected by the number, size and distribution of inclusions and the amount of hydrogen available for precipitation in the molecular state; the pressure necessary to ensure a critical stress intensity sufficient to maintain crack (cleavage) growth depends on the availability of hydrogen from the surrounding matrix. The concept of dislocations playing a part in HE has been pursued by Lynch [8] and a similar role of dislocation/hydrogen interaction affecting hydrogen embrittlement has been suggested by Tien *et al.* [17], i.e. dislocation transport of hydrogen at a much faster rate than lattice diffusion, and if this is specific to a region around an incoherent particle then this would lead to the localized brittle regions (i.e. rosettes) as local failure centres [3, 18, 19]. The final ligaments to fail, existing between the cleavage rosettes, will fail in a ductile manner after exhaustion of the hydrogen by precipitation into the inclusion sites. It would therefore be consistent that under conditions where macroscopic crack growth occurs on a broad front in a hydrogenated specimen that such an inclusion-assisted pressurization mechanism would be favoured by the presence of closely spaced inclusions [2].

5. Conclusions

1. This series of experiments has confirmed earlier work on a eutectoid plain carbon steel wire [7] that the susceptibility to HE at a given strength level is sensitively related to the microstructural state.

2. In general, the susceptibility to HE increased as the microstructures changed from ferrite–pearlite to ferrite–bainite and finally to martensite.

3. Fractography of HE ferrite–pearlite microstructures showed that fracture was transgranular and was initiated at non-metallic inclusions; small cracked volumes, called rosettes, were induced by cleavage growth around the inclusions. Load-supporting ligaments between the rosettes failed in a ductile or mixed ductile–quasi-cleavage manner.

4. HE martensitic specimens failed in a brittle intergranular manner; non-metallic inclusions were observed in fracture surfaces only when they were located at prior austenite grain boundaries, i.e. no evidence of inclusion-initiated HE failure was observed. Extensive grain-boundary triple-point cracking and occasional inter-lath cracking was observed in the martensite structures.

5. For the HE ferrite–pearlite structures (i) the fracture stress was reduced to 65% of the uncharged fracture stress; (ii) the time to failure in a slow-strain

tensile test was reduced to 65% of the uncharged time to failure; and (iii) the ductility (as measured by percentage reduction of area) was reduced to 40% of the uncharged ductility.

6. Changing the grain size from 5 to 500 μm in the HE ferrite–pearlite microstructures did not significantly alter (i) the degree of embrittlement (measured as percentage reduction of area), (ii) the fractional change in time to failure, (iii) the fractional change in fracture stress $\sigma_{F_{CH}}/\sigma_{F_U}$ and (iv) the fractional change in ultimate tensile strength $\sigma_{UTS_{CH}}/\sigma_{UTS_U}$.

7. (i) In martensitic specimens the fracture stress in the presence of hydrogen was around 30% of the uncharged fracture stress; this fracture stress decreased with increasing prior austenite grain size. (ii) Increasing the prior austenite grain size of hydrogen-charged martensitic structures from 100 to 500 μm reduced the time to failure by a half; the time to failure of charged specimens was about 25% of the uncharged specimens and the ratio of failure times $t_{F_{CH}}/t_{F_U}$ did not change with increasing grain size. (iii) The ductility of hydrogen-charged martensitic specimens (measured as a reduced reduction of area) was around 10% of the uncharged specimens; the ductility increased as prior austenite grain size increased.

References

1. F. FITZGERALD, in Proceedings of the Spring Residential Conference on Hydrogen in Steel, University of Bath, April 1982 (Institution of Metallurgists and Metals Society, London, 1982) p. 1.
2. I. M. BERNSTEIN, A. W. THOMPSON, F. GUTIERREZ-SOLANA and L. CHRISTODOULOU, in Proceedings of the 1st International Conference on Current Solutions to Hydrogen Problems in Steels, Washington, D.C., November 1982, edited by C. G. Interrante and G. M. Pressouyre (American Society for Metals, Ohio, Metals Park) p. 259.
3. A. W. THOMPSON and I. M. BERNSTEIN, in Proceedings of the Conference on Hydrogen Effects in Metals, Warrendale, March 1981, edited by I. M. Bernstein and A. W. Thompson (Metallurgical Society of AIME, New York, 1981) p. 291.
4. Y. SHUBINSKY, T. J. DAVIES and D. A. RYDER, in Proceedings of the Spring Residential Conference on Hydrogen in Steel, University of Bath, April 1982 (Institution of Metallurgists and Metals Society, London, 1982) p. 181.
5. S. A. AHMAD, D. A. RYDER and T. J. DAVIES, *Engng. Fract. Mech.* **7** (1975) 357.
6. J. D. HOBSON and C. SYKES, *J. Iron Steel Inst.* **11** (1951) 209.
7. D. A. RYDER, T. GRUNDY and T. J. DAVIES, in Proceedings of 1st International Conference on Current Solutions to Hydrogen Problems in Steels, Washington, D.C., November 1982, edited by C. G. Interrante and G. M. Pressouyre (American Society for Metals, Metals Park) p. 272.
8. S. P. LYNCH, *Acta Metall.* **1** (1984) 79.
9. I. M. BERNSTEIN and A. W. THOMPSON, in "Alloy and Microstructural Design" (Academic, New York, 1976) p. 248.
10. A. J. KUMNICK and H. H. JOHNSON, *Acta Metall.* **28** (1980) 33.
11. W. M. ROBERTSON and A. W. THOMPSON, *Met. Trans. A.* **11A** (1980) 553.
12. E. H. VAN DEVENTER, V. A. MACLAREN and V. A. MARONI, *J. Nucl. Mater.* **88** (1980) 168.
13. Kh. G. SCHMITT-THOMAS, P. M. WOLLRAB and B. HOFFMEISTER, in Proceedings of the 2nd International Congress on Hydrogen in Metals, Paris, June 1977, (Pergamon, Oxford, 1978) Paper 4A6.
14. E. STRECKER, D. A. RYDER and T. J. DAVIES, *J. Iron Steel Inst.* **12** (1969) 1639.
15. A. W. THOMPSON and I. M. BERNSTEIN, in Proceedings of the 3rd International Congress on Hydrogen and Materials, Paris, June 1982, edited by P. Azou (Pergamon, Oxford, 1982) p. 845.
16. R. A. ORIANI, *Ann. Rev. Mater. Sci.* **8** (1978) 327.
17. J. K. TIEN, S. V. NAIR and R. R. JENSEN, in Proceedings of Conference on Hydrogen Effects in Metals, Warrendale, 1980, edited by I. M. Bernstein and A. W. Thompson, (Metallurgical Society of AIME, New York) p. 37.
18. J. ALBRECHT, I. M. BERNSTEIN and A. W. THOMPSON, *Met. Trans. A* **13A** (1982) p. 811.
19. M. KURKELA and R. M. LATANISION, *Scripta Metall.* **13** (1979) 972.

Received 21 July
and accepted 22 September 1986